Transient bow shock around a cylinder in a supersonic dusty plasma

John K. Meyer and Robert L. Merlino

Additional information on Phys. Plasmas

Transient bow shock around a cylinder in a supersonic dusty plasma

John K. Meyer and Robert L. Merlino
Department of Physics and Astronomy, The University of Iowa, Iowa City, Iowa 52242, USA

Visual observations of the formation of a bow shock in the transient supersonic flow of a dusty plasma incident on a biased cylinder are presented. The bow shock formed when the advancing front of a streaming dust cloud was reflected by the obstacle. After its formation, the density jump of the bow shock increased as it moved upstream of the obstacle. A physical picture for the formation of the electrohydrodynamic bow shock is discussed. © *2013 AIP Publishing LLC*.
[http://dx.doi.org/10.1063/1.4812460]

A bow shock is formed on the upstream side of a body immersed in a supersonic flow. If the leading edge of the body is blunt, a detached bow shock is formed, while for a pointed body, the bow shock can touch the body.[1] The earth's bow shock stands upstream of the magnetopause and is formed when the supersonic solar wind flow encounters an "obstacle"—the earth's magnetic field. A bow shock slows the supersonic flow incident on an obstacle to subsonic speeds, allowing the flow to bend around it. In this note, observations of the dynamic evolution of a bow shock formed in front of an electrically biased cylinder in a supersonically flowing dusty plasma are presented. The negatively charged dust particles were decelerated and deflected by the repulsive electric field of the cylinder. A steady-state bow shock in a gravity-driven two-dimensional supersonic flow of a dusty (complex) plasma was observed by Saitou *et al.*[2] A survey of experiments on flowing dusty plasmas has been presented elsewhere.[3]

The experiments were performed in the device shown schematically in Fig. 1. A dusty plasma was formed using a DC glow discharge plasma in argon at a pressure of 140 mTorr. The glow discharge was formed on a 3.2 cm diameter disk electrode biased at $\sim$300 V with respect to the grounded walls of the vacuum chamber. The discharge current was 5 mA with a plasma density $\sim 10^{13}$–10^{14} m^{-3}. The electron and ion temperatures were 2.5 eV and 0.025 eV, respectively. A 3 mT axial magnetic field was applied to confine the electrons and produce an elongated anode glow.

1 μm diameter spherical glass particles initially on a floating tray below the anode were incorporated into the plasma when the discharge was ignited. The primary dust cloud (labeled P in Fig. 1) was stationary. The dust particles were illuminated by a thin ($\sim$1 mm) sheet of 532 nm laser light, and imaged using a Photron (FASTCAM 1024 PCI) CMOS video camera at a rate of 60 frames/s. The intensity of scattered light was directly proportional to the dust density.

A secondary dust cloud (labeled S in Fig. 1) was trapped using a grounded L-shaped mesh electrode located 15 cm from the anode. When the ground connection to the mesh was disconnected and the mesh allowed to float electrically, the trapping potential well was removed, and the secondary

cloud expanded toward the anode. Further details of the flowing dusty plasma can be found in Heinrich *et al.*[4]

A 0.5 mm diameter wire was placed downstream of the flowing secondary dust cloud and oriented with its axis perpendicular to the flow. The wire was biased at +220 V relative to ground, and the plasma potential in the vicinity of the probe was $\sim$+230 V as measured with an emissive probe. The potential on the wire was set to repel the negatively charged dust grains. If a floating or negatively biased wire is inserted into a stationary dusty plasma, a dust void is formed around the wire.[5] For the case of a flowing dusty plasma, this cylindrical void region surrounding the wire was the effective obstacle to the flow. Fig. 2 shows a series of six single-frame video images of the secondary dust cloud before and after it was released from the electrostatic trap formed by the mesh electrode. (The bright dot in the images is the wire, which appears larger than it actually was due to reflection of the laser light.) The image labeled t0 is the initial trapped dust cloud. When the cloud was released, it expanded from the lower left to the upper right toward the wire. The cloud swept over the wire by t = 0.08 s, and the first clear indication of the formation of a bow shock was observed at t = 0.1 s. As the cloud continued to stream toward the wire, the intensity of the bow shock increased and it began receding upstream, as seen in the images for t > 0.1 s. For t > 0.35 s, the bow shock began to weaken in intensity and finally disappeared when the trailing edge of the dust cloud moved downstream.

Dust density profiles at various times starting from the release of the trapped cloud are shown in Fig. 3. The dust density profiles correspond to the average light intensities along the region of interest (ROI) indicated by the 1 mm wide rectangular region shown in the t0 image of Fig. 2. The same ROI was used for all the profiles in Fig. 3. Negative distances refer to positions *upstream* of the wire, which was taken to be at the origin; times (in units of 1/60 s) correspond to video frame numbers with t = 0 taken as the time when the cloud was released. The left panel in Fig. 3 shows the progression of the advancing front toward the wire. From an analysis of the profiles in Fig. 3 and similar ones taken along slightly different ROIs, it was determined that the average velocity of the advancing front was $u_f \approx (13 \pm 4)$ cm/s. The Mach number of the dust flow was computed as M = u_f/C_{da},
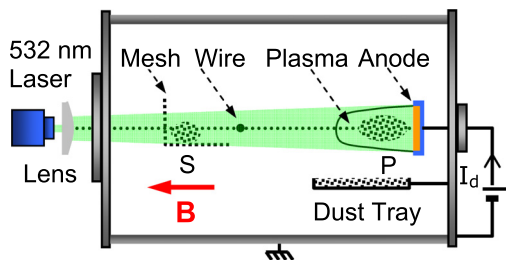
20, 074501-1

FIG. 1. Schematic of the experimental set up. P and S designate primary and secondary dust clouds.
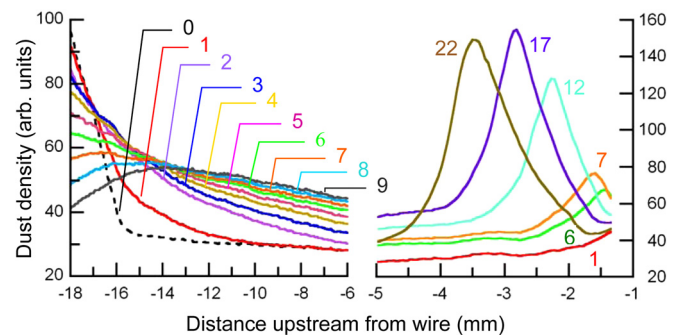

FIG. 3. Dust density profiles for various times after the release of the secondary dust cloud. The position of the wire was at 0 mm. The dust density profiles were obtained within the ROI shown in image t0 of Fig. 2. The density profile of the initial trapped cloud is shown as the dashed line. The left panel shows the advancing dust front up to t = 9/60 s after the release of the dust cloud. The right panel shows, on an expanded spatial scale, profiles of the dynamics of the bow shock, which first forms very close to the wire and then moves upstream.

where C_{da} is the dust acoustic speed, given by $C_{da} \approx \sqrt{\alpha Z_d^2 k_B T_i / m_d}$, where Z_d and m_d are the dust charge number and mass, respectively, $\alpha = n_d/n_i$ is the ratio of the dust density to ion density, and T_i is the ion temperature.[6] The electron temperature and ion density were measured with a double Langmuir probe, and the dust charge was estimated from Orbital Motion Limited (OML) charging theory to be $eZ_d \approx -2000e$, for a dust radius of 0.5 μm (dust mass $m_d \sim 10^{-15}$ kg). The dust density was estimated[4] from the video images and was in the range of $\sim 5 \times 10^9 - 1 \times 10^{10}$ m^{-3}. These estimates yield a dust acoustic speed $\sim$5–10 cm/s, or a flow Mach number, $1 < M < 3$. Supersonic dust flow was evident by the observation that dust acoustic waves, which were excited in the secondary cloud by the ion discharge current from the anode, propagated in the direction of the dust flow rather than in the direction of the ion current as observed in *stationary* dust clouds. Dust acoustic waves can be seen in the last two images of Fig. 2 in the dust flowing around the wire.

The expanding supersonic dust cloud behaved as a shock wave incident on a blunt obstacle, as shown in the profiles from t = 6/60 s to t = 22/60 s on the right panel of Fig. 3. The shock was reflected by the obstacle and developed into a bow shock as it moved upstream. The amplitude of the bow shock was characterized by the dust density jump n_{d2}/n_{d1}, where n_{d2} is the peak density in the shock and n_{d1} is the dust density upstream of the shock. The density jump ratio n_{d2}/n_{d1} was obtained from the profiles shown in Fig. 3 and reached a maximum value $\sim$4 at t = 17/60 s. The time history of the position of the bow shock from the wire and the density jump are shown in Fig. 4, where t = 0 corresponds to the time when the bow shock was first apparent (t = t0 + 0.08 s in Fig. 2). The bow shock moved upstream with a speed of 7.5 mm/s relative to the wire, increased in amplitude, and reached a maximum standoff distance of about 4 mm at t ≈ 0.3 s, after which it was swept downstream as the trailing edge of the cloud passed over the wire. The distance–time plot indicates that the bow shock never acquired a steady-state position; this was probably due to the finite size of the dust cloud.
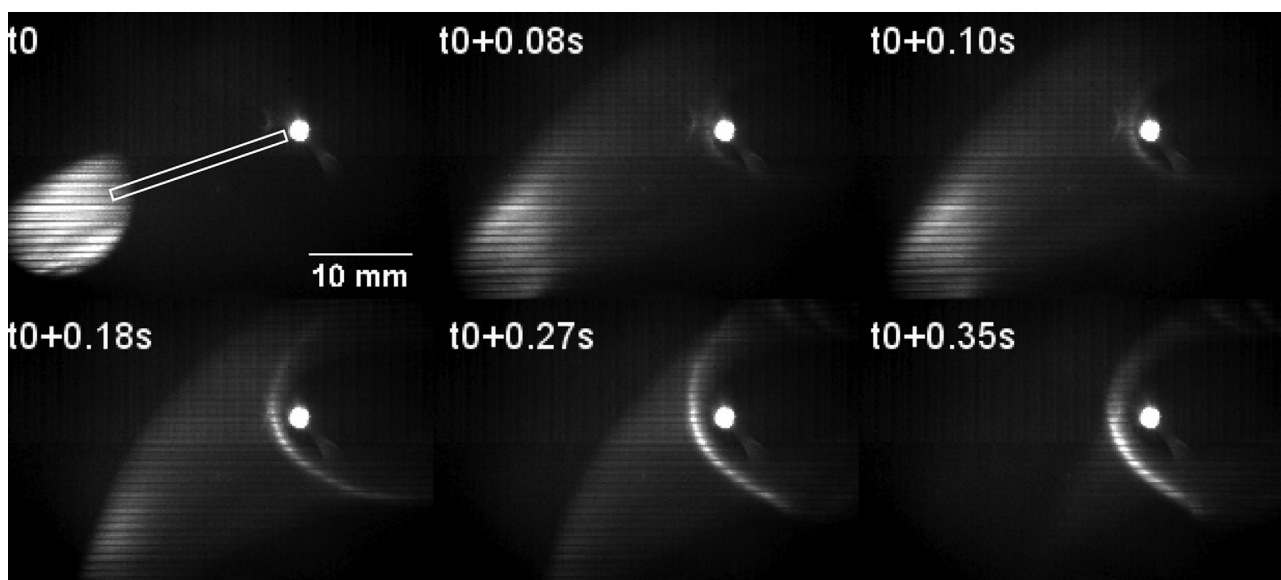

FIG. 2. A series of single-frame video images of the initial trapped secondary dust cloud (t0) and the bow shock at various times after the secondary cloud was released. The horizontal stripes in the images occur due to the laser sheet passing through the mesh. The elongated rectangular box shown in the image labeled t0 is the ROI used to obtain dust density profiles shown in Fig. 3 (enhanced online) [URL: http://dx.doi.org/10.1063/1.4812460.1].
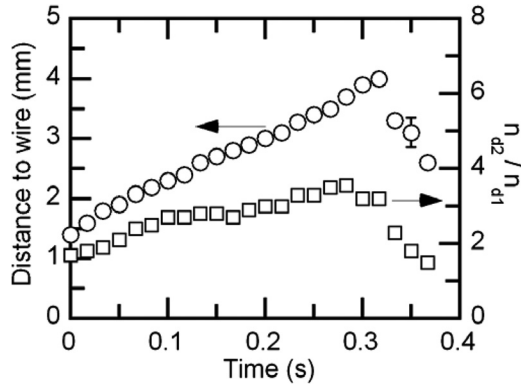
FIG. 4. Position (circles) and amplitude, n_{d2}/n_{d1} (squares) of the bow shock vs. time.

An order of magnitude estimate for the bow shock standoff distance Δ was obtained by computing the distance of closest approach of a (negative) dust particle moving toward the wire with zero impact parameter by equating the dust kinetic energy far from the wire to its electric potential energy at Δ, $m_d u_d^2/2 = eZ_d V(\Delta)$, where $V(\Delta)$ is the potential at the standoff distance. The obstacle is a cylinder of radius b and biased relative to the plasma at the potential V_0. The cylinder is negative with respect to the plasma, so it is shielded primarily by ions. For simplicity, the potential of the wire will be modeled as that of a sphere of radius b, $V(r) = (V_0 b/r)e^{-r/\lambda_{Di}}$, where λ_{Di} is the ion Debye length.[7] With $r = \Delta$, the standoff distance was computed by solving $(m_d u_d^2)\Delta - (2eZ_d V_0 b)e^{-\Delta/\lambda_{Di}} = 0$. The ion density near the wire was $n_i \approx 10^{13}\,\mathrm{m}^{-3}$, so that the Debye length was $\sim 400\,\mu m$. From the known bias on the wire and from measurements of the potential near the wire, V_0 is estimated to be in the range of a few volts. The standoff distance Δ was computed for dust speeds $u_d \approx 5\text{--}15$ cm/s, and for $V_0 \approx 1\text{--}20$ V. Over this range of parameters, the standoff distance Δ was on the order of 0.8 to 2.5 mm, comparable to the observed values.

The following physical picture of the interaction of the dust flow with the obstacle can be considered. When the cloud was initially incident on the wire, it was able to reach to within a distance on the order of the Debye length of the wire. As the dust was slowed down by the repulsive electric field, the negative charge density increased in front of the obstacle which enhanced the repulsive force, pushing the dust further upstream. The build-up of negative charge density in front of the obstacle can be seen as an effective increase in the wire potential which provides the mechanism for the reflection of the advancing shock and the formation of the bow shock. This is analogous, in the case of the earth's bow shock; to the compression of the magnetic field by the kinetic pressure of the solar wind.[8] It should be kept in mind that this simple model does not take into account a number of potentially important effects such as the variation of the ion density and temperature near the wire as well as variations in the grain charge near the wire. Numerical simulations should be performed to obtain a detailed understanding of this phenomenon.

As pointed out by Morfill *et al.*, dusty plasmas provide a "unique tool to model classical fluids."[9] The ability to study, at the kinetic level, weakly damped dust particle motion is a unique feature of dusty plasma physics research. It is interesting to note also that the flow-obstacle interaction problem has been studied, not only in connection with gas dynamic applications, such as shock tube experiments,[10] but also in granular flows where shock waves have been observed.[11]

[1]L. D. Landau and E. M. Lifshitz, *Fluid Mechanics*, 2nd ed. (Pergamon Press, Oxford, 1987).

[2]Y. Saitou, Y. Nakamura, T. Kamimura, and O. Ishihara, Phys. Rev. Lett. **108**, 065004 (2012).

[3]J. K. Meyer, J. R. Heinrich, S.-H. Kim, and R. L. Merlino, J. Plasma Phys., 1–6, doi: 10.1017/S0022377813000299 (published online 2013).

[4]J. H. Heinrich, S.-H. Kim, J. Meyer, and R. L. Merlino, Phys. Plasmas **18**, 113706 (2011).

[5]C. O. Thompson, N. D'Angelo, and R. L. Merlino, Phys. Plasmas **6**, 1421 (1999).

[6]N. N. Rao, P. K. Shukla, and M. Y. Yu, Planet. Space Sci. **38**, 543–546 (1990).

[7]No analytic model is available for the potential of a shielded cylindrical object of finite length. Rough estimates indicate that the use of cylindrical geometry would not have made a big difference in the standoff distance.

[8]R. J. Walker and C. T. Russell, "Solar wind interactions with magnetized planets," in *Introduction to Space Physics*, edited by M. G. Kivelson and C. T. Russell (Cambridge University Press, Cambridge, 1995), pp. 164–202.

[9]G. E. Morfill, M. Rubin-Zuzic, H. Rothermel, A. V. Ivlev, B. A. Klumov, H. M. Thomas, and U. Konopka, Phys. Rev. Lett. **92**, 175004 (2004).

[10]G. Patz, Acta Mech. **32**, 89–100 (1979).

[11]V. Buchholtz and T. Pöschel, Granular Matter **1**, 33–41 (1998); E. C. Rerocha, C. Bizon, M. D. Shattuck, and H. L. Swinney, Phys. Rev. Lett. **88**, 014302 (2001); X. Cui and J. M. N. T. Gray, J. Fluid Mech. **720**, 314–337 (2013).